ADVANCED MATERIALS

Supporting Information

for *Adv. Mater.*, DOI 10.1002/adma.202309862

A Fiber Sensor for Long-Term Monitoring of Extracellular Potassium Ion Fluctuations in Chronic Neuropsychiatric Diseases

Jiajia Wang, Liyuan Wang, Yiqing Yang, HongJian Li, Xinlin Huang, Ziwei Liu, Sihui Yu, Chengqiang Tang, Jiawei Chen, Xiang Shi, Wenjun Li, Peining Chen, Qi Tong, Hongbo Yu, Xuemei Sun and Huisheng Peng**

Supporting Information for

A Fiber Sensor for Long-term Monitoring of Extracellular Potassium Ion Fluctuations in Chronic Neuropsychiatric Diseases

Jiajia Wang[1], Liyuan Wang[1], Yiqing Yang[1], HongJian Li[2], Xinlin Huang[1], Ziwei Liu[1], Sihui Yu[1], Chengqiang Tang[1], Jiawei Chen[1], Xiang Shi[1], Wenjun Li[1], Peining Chen[1], Qi Tong[3], Hongbo Yu[2], Xuemei Sun[1] and Huisheng Peng[1]**

[1]*J. Wang, Dr. L. Wang, Y. Yang, X. Huang, Z. Liu, S. Yu, Dr. C. Tang, J. Chen, X. Shi, W. Li, Prof. P. Chen, Prof. X. Sun, Prof. H. Peng*

State Key Laboratory of Molecular Engineering of Polymers, Department of Macromolecular Science, Institute of Fiber Materials and Devices, and Laboratory of Advanced Materials, Fudan University; Shanghai, 200438, China.

[2]*Dr. H. Li, Prof. H. Yu*

Vision Research Laboratory, School of Life Sciences, State Key Laboratory of Medical Neurobiology, Collaborative Innovation Center for Brain Science, Fudan University; Shanghai, 200438, China.

[3]*Prof. Q. Tong*

Department of Aeronautics and Astronautics, Fudan University, Shanghai, 200433, China.

**Correspondence: sunxm@fudan.edu.cn, penghs@fudan.edu.cn.*

This file includes:

Materials and Methods

1. Materials and chemicals

Potassium ionophore (valinomycin), sodium tetrakis[3,5-bis(trifluoromethyl)phenyl] borate and tungsten (W) wire (15 and 100 μm) were purchased from Macklin Biochemical Co., Ltd. (China). Poly(vinyl chloride), tetrahydrofuran, bovine serum albumin, poly(ethylene oxide)-poly(propylene oxide)-poly(ethylene oxide) (PEO-PPO-PEO, F127), lipopolysaccharide (L-2880) and fluoxetine (F132) were purchased from Sigma-Aldrich (USA). Dioctyl sebacate, polyvinyl butyral (PVB) and multiwalled carbon nanotube (C121257) were purchased from Aladdin (China). KCl, silver (Ag) wire (100 μm) and platinum (Pt) wire (50 μm) were purchased from Alfa Aesar (USA). Poly(3,4-ethylenedioxythiophene):poly(styrenesulfonate) (PEDOT:PSS, PH1000) was purchased from Clevios (Germany). Ionic liquid (4-(3-butyl-1-imidazolio)-1-butanesulfonic acid triflate) was purchased from Santa Cruz Biotechnology (USA). Phosphate buffered saline (PBS, pH = 7.4) was purchased from Solarbio Science and Technology Co., Ltd. (China). Artificial cerebrospinal fluid was obtained from Beijing Leagene Biotechnology Co., Ltd.. Dimethylsulfoxide, isopropanol and other common reagents were purchased from Sinopharm Chemical Reagent Co., Ltd. (China). All chemical reagents were used as received.

2. Device fabrication

2.1. Fabrication of the FKS.

Carbon nanotube fibers (CNTFs) were synthesized by the floating catalyst chemical vapour deposition method[1]. Hydrophobic-treated PEDOT:PSS (HT-PP) was obtained on the surface of a CNTF via treatment with an ionic liquid and dimethylsulfoxide. First, 1.15 mg of the ionic liquid was added to 0.1 g PEDOT:PSS solution, and the mixed

solution was stirred for 30 min. Then, the prepared solution was dip-coated onto the surface of the CNTF, and the composite fiber was immersed into a mixed solution of dimethylsulfoxide and isopropanol at a 1:9 volume ratio for 30 min to remove PSS. Finally, we immersed the composite fiber into deionized water for washing. The obtained CNTF/HT-PP fiber was dried at room temperature for over 3 h. Then, 4 μL of the K^+-selective membrane solution was coated onto the CNTF/HT-PP fiber. The K^+-selective membrane solution was prepared by mixing 4.2 mg valinomycin, 1.1 mg sodium tetrakis[3,5-bis(trifluoromethyl)phenyl] borate, 68.6 mg poly(vinyl chloride) and 129.2 mg dioctyl sebacate into 2.4 mL tetrahydrofuran. The fabricated FKS was stored at 4 °C before use. The other K^+ sensors used as comparison samples were fabricated with the same procedures but different conductive substrates, e.g., tungsten wire and carbon fiber, or a different transduction layer, e.g., PEDOT:PSS.

2.2. Preparation of the Ag/AgCl reference electrode.

The Ag layer was first electrodeposited onto the CNTF in a 5×10^{-3} M $AgNO_3$/1 M KNO_3 solution by cyclic voltammetry from −0.9 to 0.9 V for 14 cycles at 100 mV s^{-1}. Chlorination was then carried out in a 0.1 M HCl/0.01 M KCl solution by cyclic voltammetry from −0.15 to 1.05 V for 4 cycles at 50 mV s^{-1}. Finally, a 2 μL PVB solution was coated onto the fiber electrode to minimize the potential drift. The PVB solution was prepared by dissolving 79.1 mg PVB, 50 mg NaCl, 2 mg PEO-PPO-PEO and 0.2 mg multiwalled carbon nanotubes into 1 mL methanol.

2.3. Preparation of the neural probe.

Through vacuum gas phase deposition (SCS Labcoter® 2, PDS 2010), 4 g parylene C was deposited onto the surface of the CNTF for insulation, and the cross-section of the fiber was obtained by laser etching. This side-insulated CNTF was used as a neural probe to record electrophysiological signals.

3. Characterization

3.1. Structure and morphology.

The structure and morphology were characterized by scanning electron microscopy (SEM, Zeiss Ultra 55) and atomic force microscopy (AFM, Bruker Fast-scan and Multimode 8). Roman spectra were measured by a laser Raman spectrometer (HORIBA JobinYvon, XploRA). X-ray photoelectron spectroscopy (XPS, Thermo Scientific K-Alpha) was carried out to analyze the elemental composition. UV–visible absorption spectrometer (Perkin-Elmer, Lambda 35) was used for measuring the stability of the transduction layer. The corresponding solutions were acquired after soaking the samples in water for 0, 6 and 24 h.

3.2. Electrochemical characterization.

All electrochemical characterizations were performed with a CHI660e electrochemical workstation (CH Instruments Ins) by using a two-electrode or three-electrode system. The two-electrode system was implemented with a K^+ sensor as the working electrode and an Ag/AgCl electrode as both the reference and counter electrodes. The three-electrode system was carried out with the K^+ sensor, Ag/AgCl and Pt as the working, reference and counter electrodes, respectively. Through a three-electrode system, cyclic voltammetry was performed in 0.1 M PBS at a scan rate of 1 V s^{-1} from −0.3 to 0.8 V. All other potentiometric experiments characterized with an open-circuit potential test program were performed by using the two-electrode system. The anti-biofouling property was verified by immersing the FKS into 10 mg mL^{-1} bovine serum albumin solution and testing every 2 hours. To compare the long-term stability, various kinds of K^+ sensors were kept in artificial cerebrospinal fluid at 37 °C and tested once a month.

3.3. Contact angle measurement.

Contact angle was measured using goniometers (Dataphysics, OCA20 and DCAT25) to calculate the surface tension and interfacial adhesion energy of the transduction layer and the K^+-selective membrane. The surface tension (γ) was calculated according to the Geometric mean equation[2],

$$(1+cos\theta)\gamma_l = 2\left[(\gamma_m^d)^{\frac{1}{2}}(\gamma_l^d)^{\frac{1}{2}} + (\gamma_m^p)^{\frac{1}{2}}(\gamma_l^p)^{\frac{1}{2}}\right] \quad (1)$$

where θ is the contact angle of a liquid on the surface, and γ_l, γ_l^d and γ_l^p are the surface tension, dispersive and polar components of the liquid, respectively. Similarly, γ_m, γ_m^d and γ_m^p are the surface tension, dispersive and polar components of the measured materials, respectively. In this study, the surface tension of deionized water ($\gamma_l = 72.1\ mJ\ m^{-2}, \gamma_l^d = 19.9\ mJ\ m^{-2}, \gamma_l^p = 52.2\ mJ\ m^{-2}$) and diiodomethane ($\gamma_l = 50\ mJ\ m^{-2}, \gamma_l^d = 47.4\ mJ\ m^{-2}, \gamma_l^p = 2.6\ mJ\ m^{-2}$) are used.

The interfacial tension between two materials ($\gamma_{m_1m_2}$) are approximated using the Geometric mean equation below,

$$\gamma_{m_1m_2} = \gamma_{m_2} + \gamma_{m_2} - 2\left[(\gamma_{m_1}^d)^{\frac{1}{2}}(\gamma_{m_2}^d)^{\frac{1}{2}} + (\gamma_{m_1}^p)^{\frac{1}{2}}(\gamma_{m_2}^p)^{\frac{1}{2}}\right] \ (\gamma_m = \gamma_m^d + \gamma_m^p) \quad (2)$$

The interfacial adhesive energy (W_a) can be calculated through equations according to Good-Girifalco theory and Geometric mean equation:

$$\gamma_{m_1m_2} = \gamma_{m_2} + \gamma_{m_2} - W_a \quad (3)$$

$$W_a = \gamma_{m_2} + \gamma_{m_2} - \gamma_{m_1m_2} = 2\left[(\gamma_{m_1}^d)^{\frac{1}{2}}(\gamma_{m_2}^d)^{\frac{1}{2}} + (\gamma_{m_1}^p)^{\frac{1}{2}}(\gamma_{m_2}^p)^{\frac{1}{2}}\right] \quad (4)$$

For a peeling process in a liquid environment, the change of associated surface energy $\Delta E_{surface}$ can be calculated as[3]:

$$\Delta E_{surface} = \left(W_a - \gamma_l\left(cos\theta_{m_1l} + cos\theta_{m_2l}\right)\right)\Delta lb \quad (5)$$

$$W^F = \Delta E_{surface} = F\Delta l \quad (6)$$

where W_a is the interfacial adhesion energy between two materials in a dry air condition, γ_l is the liquid surface tension, $\theta_{m_1 l}$ and $\theta_{m_2 l}$ are the contact angles of liquid on two materials, respectively. W^F is the work done by peeling force F with a small peeling distance Δl.

The peeling force per unit width is now written as:

$$F/b = W_a - \gamma_1\left(cos\theta_{m_1 l} + cos\theta_{m_2 l}\right) \quad (7)$$

Eq. (7) shows the relationship between peeling force per unit and contact angle of materials.

3.4. Mechanical characterization.

Young's moduli of different materials were measured by nanoindentation (Agilent Technologies Singapore Sales Pte. Ltd.)

4. Finite element analysis

4.1. Stress simulation under bending.

Three-dimensional finite element analysis models were established to simulate the stress distribution under bending for various fiber materials with the same dimensions (0.05 mm in diameter and 1 mm in length). The mechanical parameters of different materials were obtained from nanoindentation experiments and previous reports[1, 4], including those of brain tissue (Young's modulus, 9 kPa; Poisson's ratio, 0.5), W wire (Young's modulus, 39.81 ± 4.86 GPa; Poisson's ratio, 0.28), carbon fiber (Young's modulus, 5.40 ± 1.01 GPa; Poisson's ratio, 0.3) and the CNTF (Young's modulus, 65.2 ± 8.81 MPa; Poisson's ratio, 0.3). The stress simulations were implemented by the commercial software package ABAQUS. In the simulations, one end of the fiber was fixed, and the other end was set free to deflect. A small-distance *L* displacement

perpendicular to the axis direction was applied at the free end of the fiber material to obtain the stress distribution.

4.2. Brain micromotion simulation.

Three-dimensional finite element analysis models were established to evaluate the mechanical matching property between fiber materials and brain tissue during micromotion. The sizes of the fiber materials were set to be the same (0.05 mm in diameter and 1 mm in length), but with different moduli. The brain was set as an isotropic neo-Hooke material with a shear modulus of 5.5 kPa. The simulations were implemented by the commercial software package ABAQUS. Before micromotion, the top of the implanted fiber material was fixed, and the other end in the tissue was set free for deflection. Then, a 50 μm displacement was laterally loaded onto the bottom surface of the brain tissue to simulate brain micromotion. The interface interaction between brain tissue and the implanted fiber material was set as friction with a friction coefficient of 0.3.

5. Animal experiment

5.1. Animals.

All animals (ICR, 8 weeks old, male) were purchased from Shanghai SLAC Laboratory Animal Co., Ltd. (certificate number: SYXK-Hu-2017-0008). The experimental protocols were approved by the Animal Experimentation Committee of Fudan University (certificate number: SYXK2020-0032). All of the animal procedures were carried out following the guidelines for the care and use of experimental animals described by the National Institutes of Health and Fudan University.

5.2. Implantation of the FKS into the mouse brain.

During the surgeries, all mice were anesthetized with 1.5% isoflurane mixed in air and fixed in a stereotactic frame (RWD Life Science Co., Ltd.). Then, the scalp was sheared off, and the connective tissues were cleaned from the skull. The implantation site was located in the hippocampus (AP, −2 mm from the bregma; ML, −1.5 mm; DV, −2.0 mm

from the surface of the skull) or lateral habenula (AP, −1.6 mm from the bregma; ML, −0.6 mm; DV, −2.6 mm from the surface of the skull). The skull at the implantation site was drilled with a hole of approximately 2 mm using a dental drill. The assisted implantation method was applied for implanting the flexible FKS and neural probe. The FKS and neural probe were adhered to the surface of tungsten wire with dissolvable gelatine and implanted. After implantation for 20 min, the gelatine was dissolved, and the assistant tungsten wire was removed from brain tissue. Then, the bare brain tissue was covered with a layer of agar gel (0.6 wt%), and the FKS and neural probe were stably fixed on the skull with dental cement adhesive (Super Bond C&B, SUN MEDICAL). The Ag/AgCl reference electrode was implanted near the FKS, and flat-heat screws were screwed to the metencephalon as the ground and reference electrode of the neural probe.

5.3. Recording of electrophysiology and extracellular K^+ *in vivo*.

For the recording of the extracellular K^+ concentration ($[K^+]_e$), the implanted FKS and Ag/AgCl electrode were connected to a CHI660e electrochemical workstation as described *in vitro*. The neural probe and its ground electrode were connected to an electrophysiological recording instrument (Cereplex Direct, Blackrock Microsystems). The recording was performed after the mice had recovered from surgery for two weeks. The anesthesia model was established by switching the anesthetic concentration between 2.0% and 0.5%, which is the volume ratio of isoflurane and air ($V_{isoflurane}$: V_{air}). All mice were fixed in a stereotaxic frame and placed in a shielded cage to prevent electromagnetic interference during the recording process. Baseline correction was performed on the potential curve recorded by the FKS *in vivo* to obtain the change in potential ($\Delta E_{[K^+]_e}$) in response to fluctuations in $[K^+]_e$. For the FKS with a sensitivity of 52.8 mV per decade, a $\Delta E_{[K^+]_e}$ of 1 mV suggested a 4.5% change in $[K^+]_e$. The mean slopes of the recorded potential curves were calculated every ten seconds to identify the change time. Correspondingly, the firing rates (10 s) of electrophysiology signals were counted. To validate the long-term stability of the FKS *in vivo*, the test was

performed once every two weeks, and the data for three mice were simultaneously recorded.

6. Depression model and behavioral assay

6.1. Tail suspension test (TST).

The test was performed using tail suspension hardware (Shanghai Yuyan Instruments Co., Ltd.). The mouse was suspended from a horizontal bar at a height of 30 cm by affixing tape to the mouse tail 2 cm from the tip. The test was conducted under normal light with a total time of 6 min. The process was recorded, and the struggle time/immobile duration in the last 4 min was quantified by tail suspension software[5] (JLBehv-FS/STGM-1).

6.2. Forced swimming test (FST).

Forced swimming hardware (Shanghai Yuyan Instruments Co., Ltd.) was used. Mouse was individually placed in a cylinder (height: 30 cm; diameter: 14 cm) containing 14 cm of water (23 ± 2 °C) and swam for 6 min. The process was videotaped and the struggle time/immobile duration in the last 4 min was analyzed by forced swimming software (JLBehv-FS/STGM-1).

6.3. Lipopolysaccharide-induced depression.

Six-weeks old mice were implanted with the FKS and neural probe with the same surgery procedures, then the mice were recovered for 14 days. Lipopolysaccharide was diluted in sterile 0.9% saline and intraperitoneally administered to mice in the experimental group at a dose of 0.5 mg kg^{-1} daily for 9 days at approximately 10 a.m.to induce depression. Subsequently, fluoxetine dissolved in sterile 0.9% saline was intraperitoneally injected at a dosage of 20 mg kg^{-1} daily for 15 days to relieve depression. The mice in the control group were injected with 0.9% saline at the same time over the entire course. During the depression process, the TST and $[K^+]_e$ fluctuations measurements were carried out on the mice in the control and experimental groups before injection and after injection of lipopolysaccharide or 0.9% saline for 1,

3, 5 and 7 days. Afterwards, the TST and $[K^+]_e$ fluctuations measurements were also carried out after the treatment with fluoxetine or 0.9% saline for 15 days. Besides, each experiment was implemented on three mice and all the mice in the control and experimental groups were placed and fed in the same environment during the whole process to avoid additional interference.

6.4. Unpredictable chronic mild stress.

Various unpredictable chronic mild stressors were sequentially delivered to the mice for 4 weeks to induce chronic depression as follows[5]: food deprivation for 12 h, water deprivation for 12 h, tail clamping with hemostatic forceps for 1 min, night illumination for 12 h, wet bedding material exposure for 12 h, physical restraint for 3 h, 46 °C treatment for 5 min and swimming in cold water at 10 °C for 6 min. The procedures were repeated every 4 days. In contrast, mice in the control group were exposed to the normal environment over the whole process.

7. Immunohistochemistry

After implanting FKS for 1 month, mice were anesthetized with 5.0% isoflurane mixed in air and then euthanized to remove the brain tissues. The brain tissues were fixed with 4% paraformaldehyde solution overnight and then embedded with paraffin to obtain brain slices with a thickness of ~4 μm. Therewith, immunofluorescence staining was conducted according to the standard procedures. For the immunofluorescence staining of astrocytes and microglia, anti-glia fibrillary acidic protein antibodies (anti-GFAP,1:1000, GB11096, Servicebio) or anti-ionized calcium binding adaptor molecule-1 antibodies (anti-Iba1, 1:200, GB13105-1, Servicebio) and anti-neuronal nuclei protein antibodies (anti-NeuN, 1:500, GB13138-1, Servicebio) were used as the primary antibodies. Cy3 conjugated goat anti-rabbit lgG(H+L) (1:300, GB21303, Servicebio) and Alexa Fluor® 488-conjugated goat anti-mouse lgG (1:400, GB25301, Servicebio) were used as the secondary antibodies. 4′6-diamidino-2-phenylindole (DAPI, G1012, Servicebio) was implemented to stain the nuclei of all cells. A scanner (NIKON ECLIPSE C1 and NIKON DS-U3) was applied to acquire the fluorescence

images.

8. Statistical analysis

The statistical analysis was conducted with Origin and Excel. The results are presented as the mean ± s.d.. The statistical tests, replicate number, error bars and *P*-values are indicated in the figure legends.

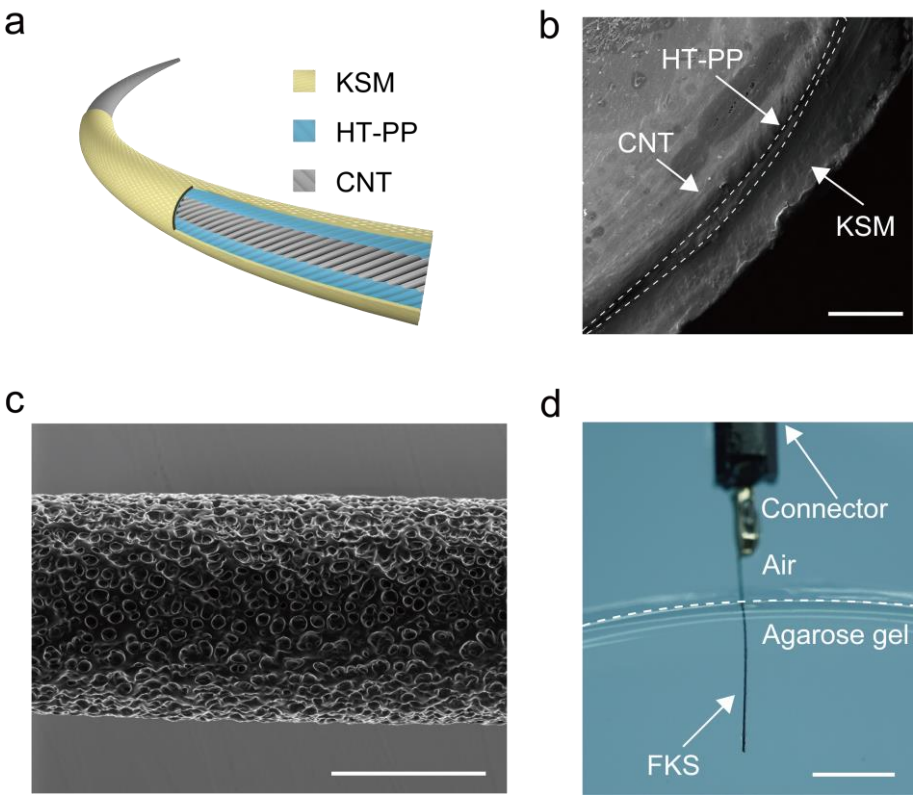

Figure S1. Structure characterization of the FKS. a) Schematic structure of the FKS. KSM represents the K^+-selective membrane. b) Scanning electron microscopy (SEM) image of the cross-section of the FKS showing a three-layer structure. Scale bar, 10 μm. c) Side-view SEM image of the FKS showing the porous surface. Scale bar, 50 μm. d) Photograph of the FKS implanted in a 0.6% agarose gel demonstrating minimal invasion. Scale bar, 3 mm.

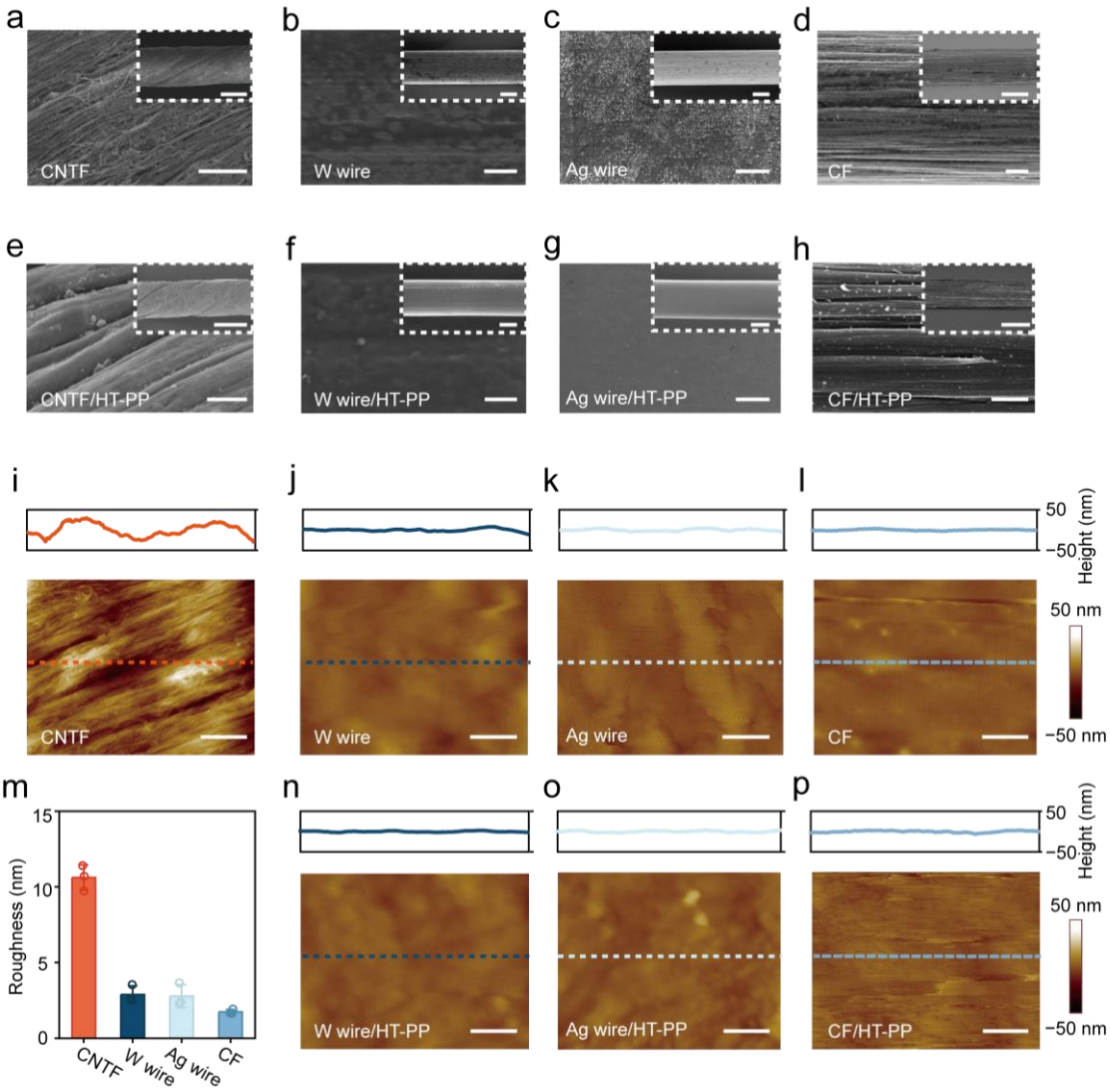

Figure S2. Surface morphologies of conductive substrates before and after the modification of HT-PP layer. a–d) SEM images of the bare conductive substrates, including the CNTF (a), W wire (b), Ag wire (c) and CF (d), at low (inset) and high magnifications. The surface of the CNTF is rougher than that of the other substrates due to the twisted structure of the carbon nanotubes. Scale bars, 50 μm (a–c), 5 μm (d) and 1 μm (a–d, inset). e–h) SEM images of the HT-PP layer on different conductive substrates, including CNTF/HT-PP (e), W wire/HT-PP (f), Ag wire/HT-PP (g) and CF/HT-PP (h), at low (inset) and high magnifications. CNTF/HT-PP possesses the highest roughness. Scale bars, 50 μm (e-g), 5 μm (h) and 1 μm (e–h, inset). i–l) AFM images (bottom panel) and height curves (top panel) of the bare conductive substrates, including the CNTF (i), W wire (j), Ag wire (k) and CF (l). The CNTF shows the

maximum height difference. Scale bars, 600 nm (i) and 200 nm (j–l). m) Roughness of the bare conductive substrates (n=3, mean ± s.d.). The CNTF possesses a much rougher surface than the other conductive substrates. n–p) AFM images (bottom panel) and height curves (top panel) of different conductive substrates modified with the HT-PP layer, including W wire/HT-PP (n), Ag wire/HT-PP (o) and CF/HT-PP (p). Scale bar, 200 nm.

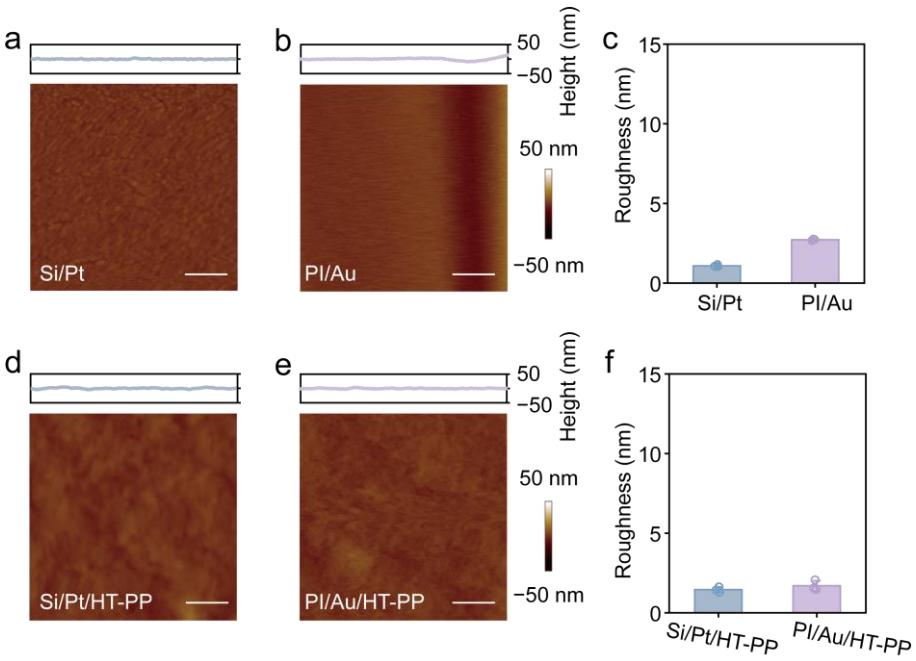

Figure S3. Roughness of the planar conductive substrates before and after the modification of HT-PP. a, b) AFM images (bottom panel) and height curves (top panel) of the bare planar conductive substrates, including the silicon with platinum layer (Si/Pt) (a) and polyimide with gold layer (PI/Au) (b). Scale bar, 200 nm. c) Roughness of the bare planar conductive substrates (n=3, mean ± s.d.). d, e) AFM images (bottom panel) and height curves (top panel) of different planar conductive substrates modified with the HT-PP layer, including Si/Pt/HT-PP (d) and PI/Au/HT-PP (e). Scale bar, 200 nm. f) Roughness of the planar conductive substrates modified with the HT-PP layer (n=3, mean ± s.d.).

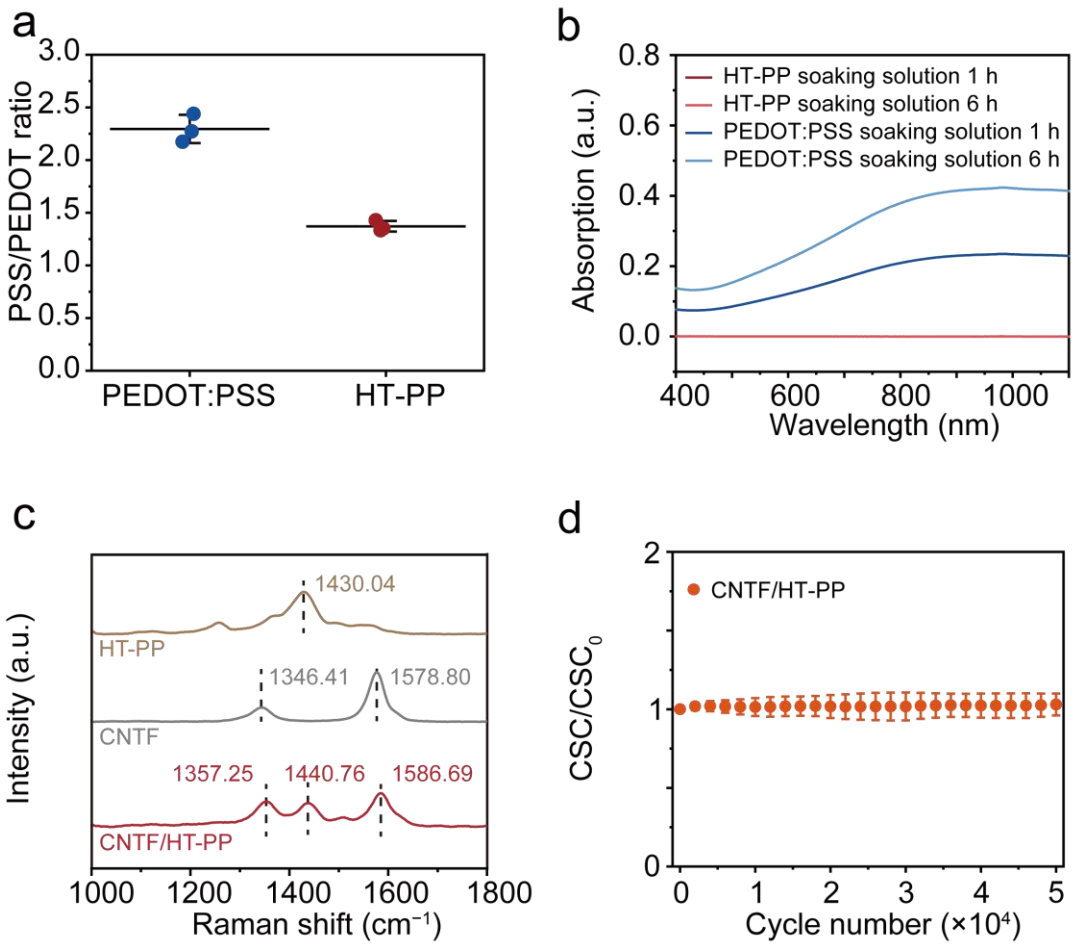

Figure S4. Stability characterization of the FKS. a) PSS/PEDOT ratio of original PEDOT:PSS and HT-PP calculated from X-ray photoelectron spectroscopy. HT-PP shows a decreased PSS ratio compared with PEDOT:PSS (n=3, mean ± s.d.). b) UV–visible spectra of the solutions in which PEDOT:PSS and HT-PP were soaked for 1 and 6 h, exhibiting the water stability of HT-PP. c) Raman spectra of pristine HT-PP, the CNTF and CNTF/HT-PP. CNTF/HT-PP demonstrates an obvious blueshift of characteristic peaks compared to pristine HT-PP and the CNTF because of the π-π interaction between them. d) Stable charge storage capability (CSC) of CNTF/HT-PP from 50,000 cyclic voltammetry cycles in phosphate buffered saline at a 1 V/s scan rate (n = 3, mean ± s.d.).

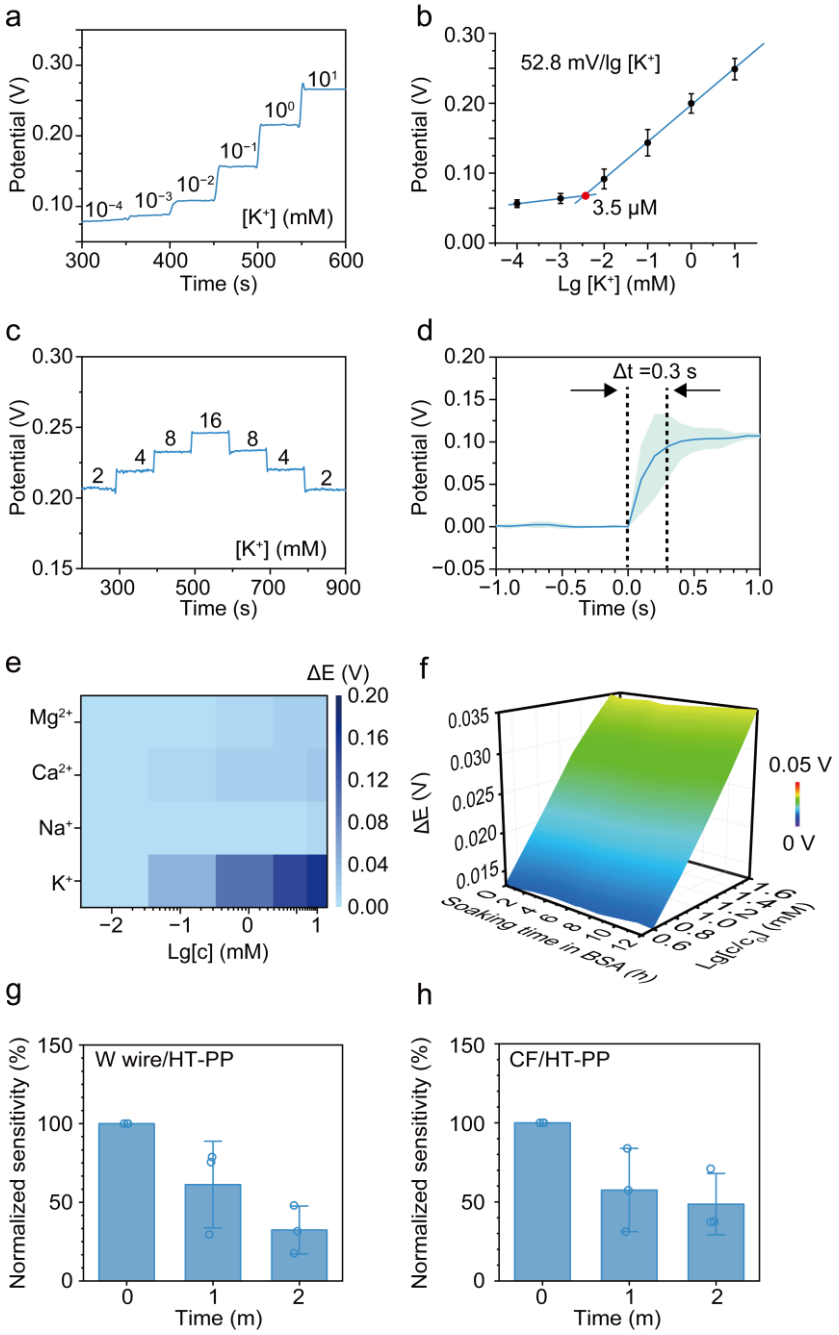

Figure S5. Sensing performance of the FKS. a) Potential responses (*vs.* Ag/AgCl) of the FKS to K^+ concentrations ranging from 0.1 μM to 10 mM. b) Sensitivity and detection limit derived from potential responses of the FKS (n = 3). c) Reversibility test of the FKS performed by recording the potential responses (*vs.* Ag/AgCl) to K^+ concentrations varied from 2 to 16 mM and back to 2 mM. The FKS shows a reversible potential. d) Response time of the FKS to K^+ concentrations varied from 0 to 0.5 mM (n = 3). The time of the potential to reach 90% of the equilibrium potential was

calculated as the temporal resolution. Light blue shading indicates the statistical s.d. and the blue curve represents the averaged potential response. e) Color map of the potential changes (ΔE, *vs.* Ag/AgCl) of the FKS in response to K^+ and the other interfering ions (Na^+, Mg^{2+} and Ca^{2+}), demonstrating high selectivity. f) 3D surface plot of the potential changes (ΔE, *vs.* Ag/AgCl) of the FKS in response to different K^+ concentrations when soaked in 10 mg mL^{-1} BSA solution for 12 h. The result presents the anti-biofouling ability. The K^+ concentration ranged from 0.5 to 21.5 mM, and the test was carried out every 2 h. g, h) Normalized sensitivities of the W wire/HT-PP-based K^+ sensor (g) and CF/HT-PP-based K^+ sensor (h) kept in artificial cerebrospinal fluid at 37 °C for 2 months, demonstrating decreased sensitivities (n = 3 for each type of K^+ sensor, mean ± s.d.).

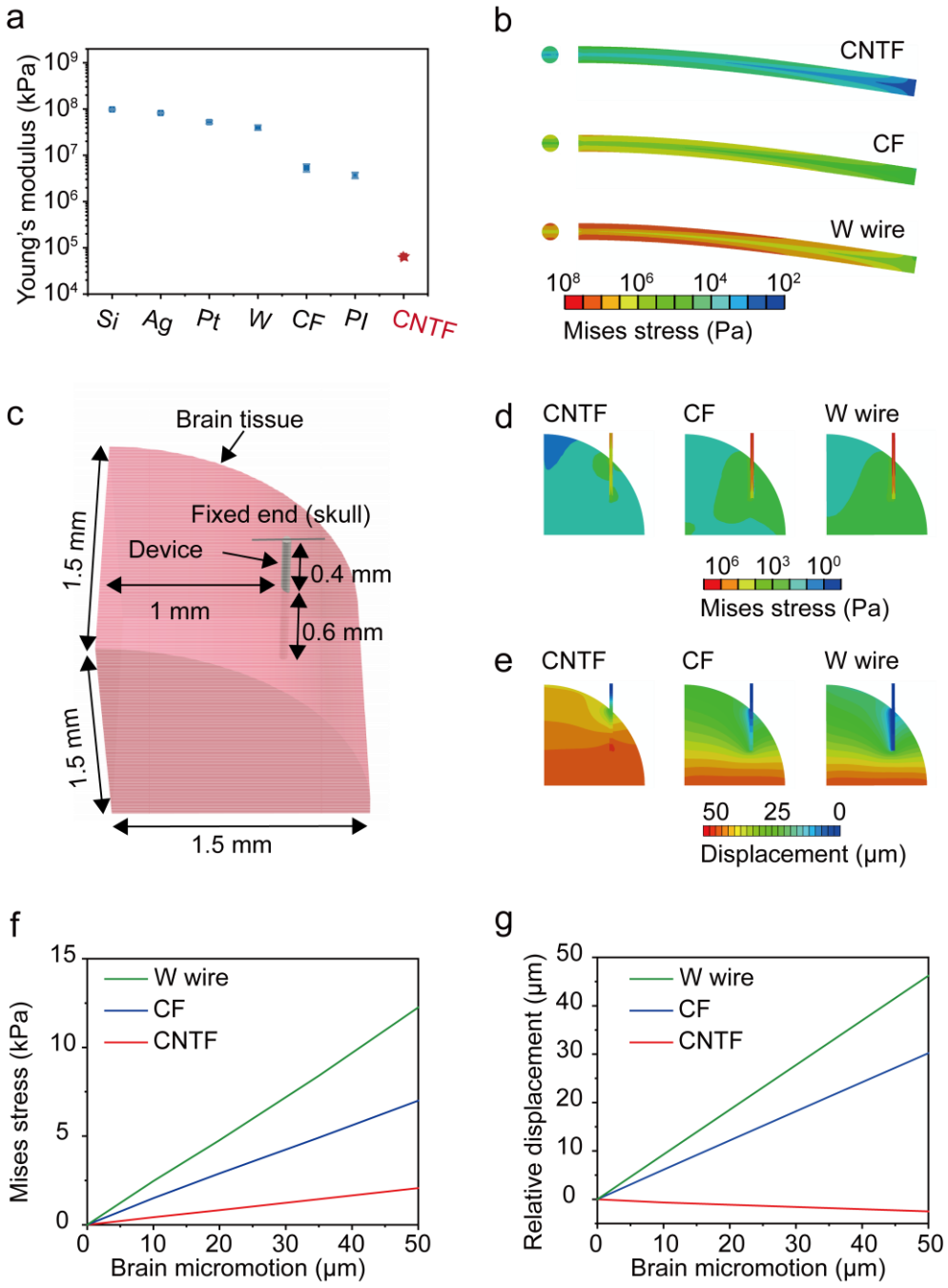

Figure S6. Mechanical analysis of the CNTF and the other substrates used in K^+ sensors. a) Comparison of the Young's moduli of the CNTF and other substrates, including Si, Ag wire, Pt wire, W wire, CF and PI (n = 5, mean ± s.d.). b) von Mises stress profiles for the CNTF, CF and W wire under slight bending deformations. The CNTF shows the smallest internal stress. c) Schematic illustration of the finite element analysis model of the brain tissue implanted with a fiber fixed to the skull during brain micromotion. d, e) von Mises stress (d) and displacement (e) profiles within the brain tissue for the CNTF,

CF and W wire under 50 μm lateral micromotion of the brain tissue. f) von Mises stress at the maximal stress point at the interface of the brain tissue and CNTF, CF or W wire during 50 μm lateral micromotion. g) Relative displacement between the brain and the bottom center of the CNTF, CF or W wire during 50 μm lateral micromotion. The stress at the interface of the CNTF and the brain tissue is much lower than that for the other substrates, and the CNTF shows consistent micromotion with the brain tissue.

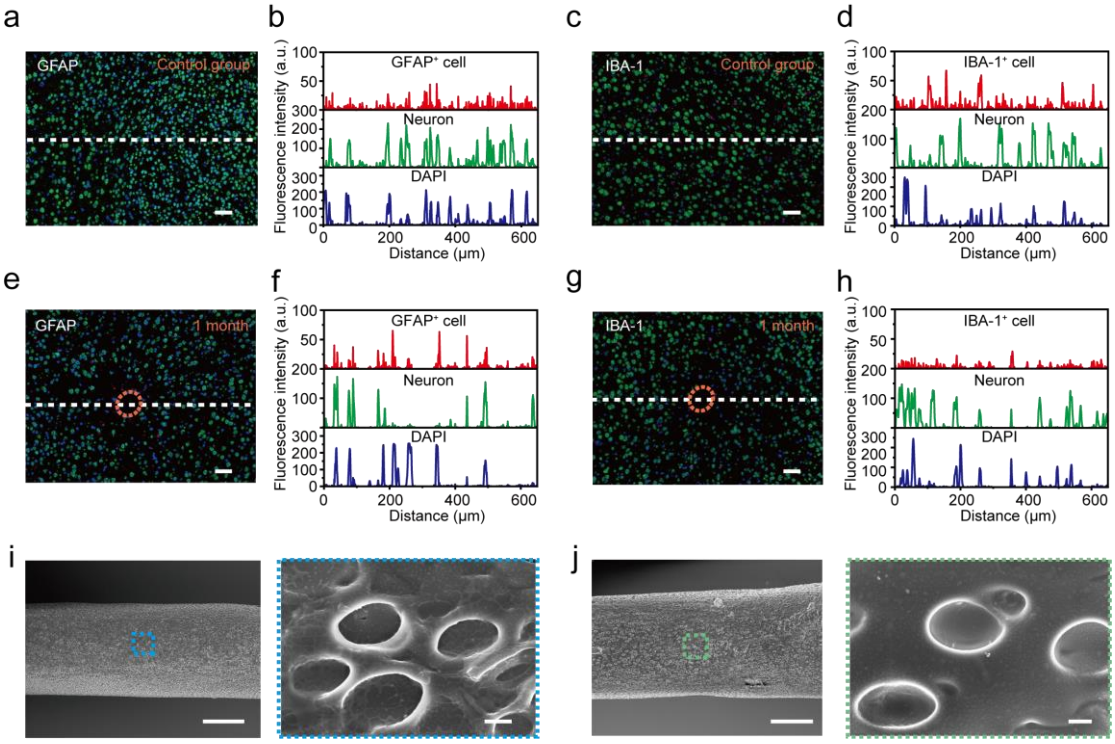

Figure S7. Biocompatibility characterization of the FKS. a–d) Merged immunohistochemical fluorescence images (a, c) and fluorescence intensity plots along the dashed white lines (b, d) of mouse brain slices in the control group at horizontal sections. Scale bar, 50 μm. e–h) Merged immunohistochemical fluorescence images (e, g) and fluorescence intensity plots along the dashed white lines (f, h) of mouse brain slices implanted with the FKS for 1 month at horizontal sections. The FKS implantation site is indicated with a dashed orange circle. The astrocytes and activated microglia were labelled with GFAP (red) and Iba1 (red), respectively; neurons were labelled with NeuN (green), and nuclei were labelled with DAPI (blue). Scale bar, 50 μm. i, j) SEM images of the FKS at low and high magnifications at 3 (i) and 6 (j) months after implantation showing no obvious protein absorption. Scale bars, 50 μm (left) and 1 μm (right).

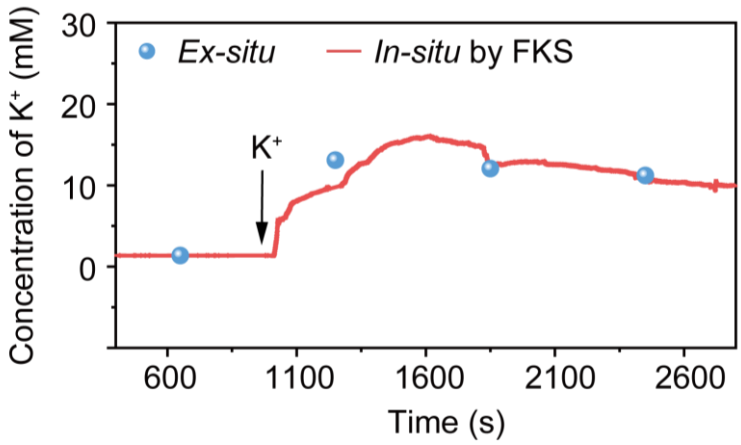

Figure S8. Consistence of the potassium ion levels between *ex-situ* analysis using potassium assay kit and *in-situ* real-time recording by FKS. FKS was implanted *in vivo* to measure the potassium ion level *in-situ* and the interstitial fluid at the implantation site was collected at a certain interval for the *ex-situ* measurement.

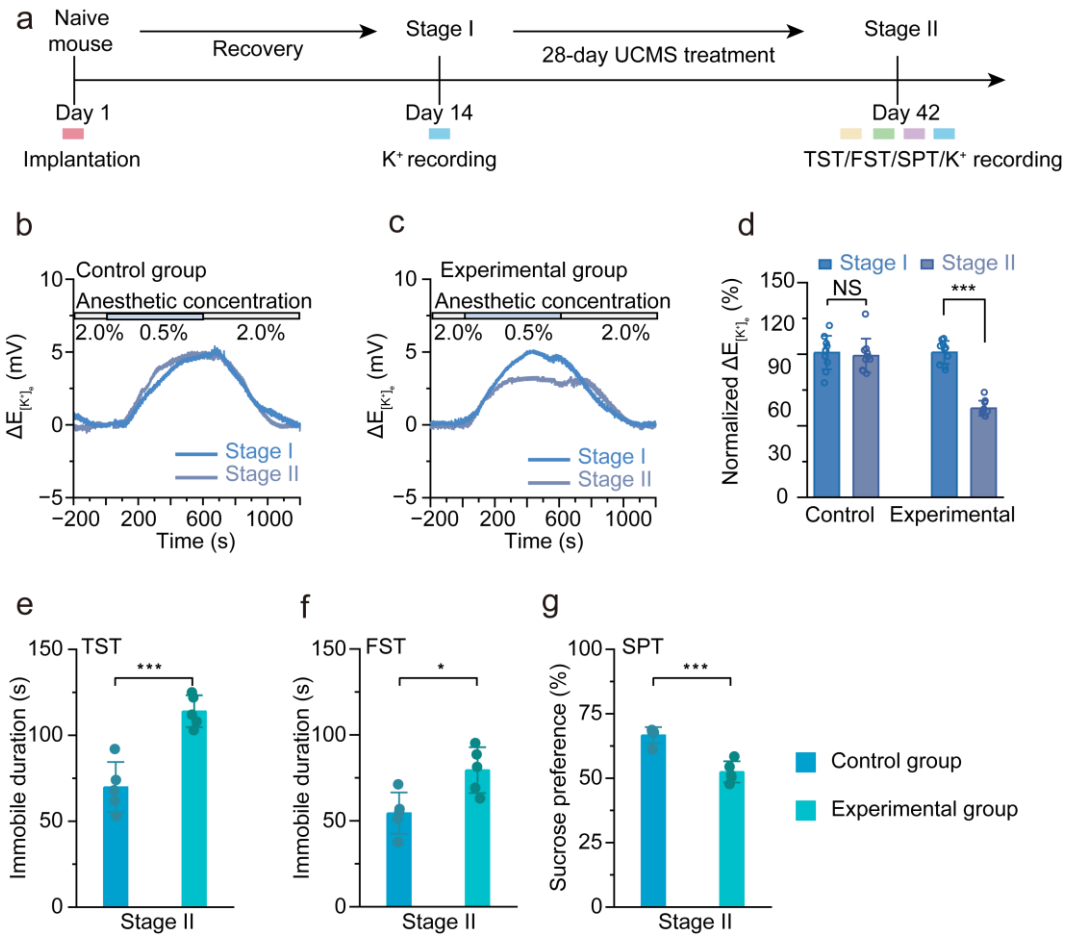

Figure S9. FKS recorded $[K^+]_e$ fluctuations under anesthetic during the development and treatment of depression. a) Experimental paradigm for the unpredictable chronic mild stress (UCMS) induced depression model. b, c) $\Delta E_{[K^+]_e}$ of the FKS in Stages I and II in the control (b) and experimental (c) groups upon varying the anesthetic concentrations. The recorded $\Delta E_{[K^+]_e}$ decreases in Stage II in the experimental group but remains stable in the control group. d) Normalized $\Delta E_{[K^+]_e}$ in Stages I and II in the control and experimental groups (n = 10 from five individual mice for each group, mean ± s.d.). *P*-values: control group: 0.6914, experimental group: $1.1876*10^{-7}$. e–g) Behavioral test data recorded from the TST (e), FST (f) and SPT (g) to evaluate the depression level (control group, n = 5; experimental group, n = 5; mean ± s.d.). *P*-values: TST: $4.5466*10^{-4}$, FST: 0.0143, SPT: $1.7572*10^{-4}$. Compared to the control group, mice in the experimental group showed apparent depression symptoms of a longer immobile

duration and a lower sucrose preference. *P*-values are calculated by one-way ANOVA analysis: NS, not significant; *P <0.05; **P<0.01; ***P <0.001.

Table S1. Temporal resolution, size and lifetime *in vivo* for $[K^+]_e$ monitoring tools in the brain.

Method	Temporal resolution	Size	Lifetime	Ref.
Microdialysis	68 s	/	1–5 d	*J. Cereb. Blood. Flow. Metab.* **2017**, 37, 1883.
Microdialysis	15 min	0.5 mm (diameter)	~6 h	*J. Neurosurg.* **2002**, 97, 97.
Droplet-based monitoring system	50 s	250 μm (diameter)	25 min	*Nat. Commun.* **2017**, 8, 1239.
Fluorescence nanosensor	1.13 s	~30 nm nanoparticle /200 μm optical fiber	30 min	*Nat. Nanotechnol.* **2020**, 15, 321.
Near-infrared nanosensor	1 s	~ 85 nm	1 h	*Sci. Adv.* **2020**, 6, eaax9757.
Glassy liquid-contact K^+ sensor	1 s	2 μm	40 min	*Nat. Neurosci.* **2014**, 17, 694.
Glassy liquid-contact K^+ sensor	1 s	2–3 μm	~2 h	*Science* **2016**, 352, 550.
Solid-contact K^+ sensor	~0.63 s	76.2 μm	6 h	*Anal. Chem.* **2016**, 88, 8942.
Solid-contact K^+ sensor	**<** 1 s	15 μm	4 d	*Angew. Chem. Int. Ed.* **2020**, 59, 10426.
Fiber K^+ sensor (FKS)	**0.3 s**	**1–100 μm**	**6 m**	**This work**

Table S2. Typical timescales of $[K^+]_e$ related chronic neuropsychiatric disease model of animals.

Neuropsychiatric diseases	**Timescale**	**Ref.**
Alzheimer's diseases	1–25 months	*Nat. Commun*. **2022**, 13, 886; *Nat. Commun*. **2022**, 13, 998; *Nat. Neurosci*. **2022**, 25, 688.
Parkinson's diseases	3 weeks–10 months	*Nature* **2020**, 582, 550.
Depression	1–5 weeks	*Nat. Commun*. **2021**, 12, 6937; *Nat. Commun*. **2022**, 13, 5462; *Nat. Commun*. **2022**, 13, 2650; *Nat. Commun*. **2022**, 13, 3544.
Huntington's diseases	2 weeks–12 months	*Nat. Biotechnol*. **2016**, 34, 838; *Nat. Commun*. **2016**, 7, 11251; *Nat. Neurosci*. **2014**, 17, 694; *Nat. Commun*. **2016**, 7, 12646; *Nat. Med*. **2014**, 20, 536.

Table S3. Typical conductive substrates and transduction layers for implantable ion sensors.

Target ion	Conductive substrate	Transduction layer	Ref.
H^+	Carbon fiber	/	*Anal. Chem.* **2016**, 88, 11238.
Ca^{2+}	Carbon fiber	Shelled hollow carbon nanospheres	*Anal. Chem.* **2019**, 99, 4421.
Ca^{2+}	Carbon fiber	Au nanoparticles	*Angew. Chem. Int. Ed.* **2021**, 60, 14429.
Ca^{2+}	Carbon fiber	/	*Chinese J. Anal. Chem.* **2019**, 47, 347.
K^+	Carbon fiber	Graphdiyne oxide-MnO_2	*Sci. China. Chem.* **2019**, 62, 1414.
K^+	Ag wire	Ag/AgCl	*Anal. Chem.* **2016**, 88, 8942.
K^+, Ca^{2+}, Na^+, H^+	W wire	Electrodeposited PEDOT:PSS	*Angew. Chem. Int. Ed.* **2020**, 59, 10426.
Ca^{2+}	Polyimide film with Au layer	Dip-coated PEDOT:PSS	*Adv. Funct. Mater.* **2020**, 2002644.
K^+	Si wafer with platinum layer	Electrodeposited PEDOT:PSS	*Sens. Actuators B Chem.* **2015**, 207, 945.
K^+	**CNTF**	**HT-PP**	**This work**

Table S4. Contact angles of different materials with water and diiodomethane (n = 3, mean ± s.d.).

Material	Water (°)	Diiodomethane (°)
PEDOT:PSS	50.67 ± 2.47	28.54 ± 1.45
HT-PP	58.9 ± 2.76	31.23 ± 0.99
W wire/HT-PP	95.12 ± 8.41	69.42 ± 3.47
Ag wire/HT-PP	111.03 ± 3.75	50.64 ± 1.90
CF/HT-PP	121.68 ± 5.29	51.34 ± 5.06
CNTF/PEDOT:PSS	116.47± 3.83	55.94 ± 5.41
CNTF/HT-PP	135.52 ± 3.71	66.05 ± 0.20
K^+ selective membrane	89.13 ± 1.15	11.55 ± 1.45

Table S5. Water contact angles of different transduction materials modified on the surface of CNTF (n = 3, mean ± s.d.).

Transduction layer	Contact angle (°)
Ag/AgCl	114.71 ± 6.91
Au nanoparticles	128.22 ± 2.66
Electrodeposited PEDOT:PSS	69.18 ± 10.26
Dip-coated PEDOT:PSS	116.47± 3.83
HT-PP	**135.52 ± 3.71**

Supplementary Reference

[1] L. Wang, S. Xie, Z. Wang, F. Liu, Y. Yang, C. Tang, X. Wu, P. Liu, Y. Li, H. Saiyin, S. Zheng, X. Sun, F. Xu, H. Yu, H. Peng, *Nat. Biomed. Eng.* **2020**, 4, 159.

[2] a) E. N. Dalal, *Langmuir* **2002**, 3, 1009; b) J. K. Park, J. D. Eisenhaure, S. Kim, *Adv. Mater. Interfaces.* **2018**, 6, 1801524.

[3] J. K. Park, Y. Zhang, B. Xu, S. Kim, *Nat. Commun.* **2021**, 12, 6882.

[4] S. Park, H. Yuk, R. Zhao, Y. S. Yim, E. W. Woldeghebriel, J. Kang, A. Canales, Y. Fink, G. B. Choi, X. Zhao, P. Anikeeva, *Nat. Commun.* **2021**, 12, 3435.

[5] a) S. Liu, J. Xiu, C. Zhu, K. Meng, C. Li, R. Han, T. Du, L. Li, L. Xu, R. Liu, W. Zhu, Y. Shen, Q. Xu, *Nat. Commun.* **2021**, 12, 6937; b) H. Yu, L. Chen, H. Lei, G. Pi, R. Xiong, T. Jiang, D. Wu, F. Sun, Y. Gao, Y. Li, W. Peng, B. Huang, G. Song, X. Wang, J. Lv, Z. Jin, D. Ke, Y. Yang, J. Z. Wang, *Nat. Commun.* **2022**, 13, 5462.